# In-Vacuum Projection of Nanoparticles for On-Chip Tunneling Spectroscopy

**Qian Yu,[†] Limin Cui,[†,‡] Nicolas Lequeux,[†] Alexandra Zimmers,[†] Christian Ulysse,[§] Valentina Rebuttini,[⊥,#] Nicola Pinna,[⊥,#] and Hervé Aubin[†,*]**

[†]Laboratoire de Physique et d'Etude des Matériaux, UMR 8213, ESPCI-ParisTech-CNRS-UPMC, 10 Rue Vauquelin, 75231 Paris, France, [§]Laboratoire de Photonique et de Nanostructures, CNRS, Marcoussis, France, [⊥]Department of Chemistry, CICECO, University of Aveiro, 3810-193 Aveiro, Portugal, and [#]Institut für Chemie, Humboldt-Universität zu Berlin, Brook-Taylor-Straße 2, 12489 Berlin, Germany. [‡]Present address: Beijing National Laboratory for Condensed Matter Physics, Institute of Physics, Chinese Academy of Sciences, Beijing 100190, China.

**ABSTRACT** Starting with a discussion of the percolation problem applied to the trapping of conducting nanoparticles between nanometer-spaced electrodes, we show that a good strategy to trap a single nanoparticle between the electrodes is to prepare chips with low coverage of nanoparticles to avoid percolating current paths. To increase the probability of trapping a single nanoparticle, we developed a new method where nanoparticles are projected in-vacuum on the chip, followed by a measure of the tunnel current, in a cycle that is repeated up to a few thousand times until a preset threshold value is reached. A plot of the tunneling current as a function of time allows discriminating between the two possible current paths, *i.e.*, a single nanoparticle trapped between the electrodes or a percolating path across many nanoparticles. We applied the method to prepare chip circuits with single gold nanoparticles, as demonstrated by the observation of Coulomb blockade. Furthermore, we applied the method to trap single magnetite nanoparticles for the study of electric-field-induced switching from insulator to metal in single nanoparticles.

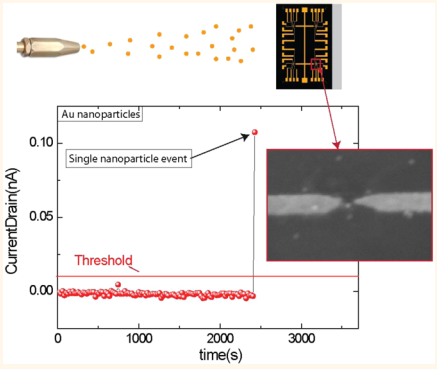


**KEYWORDS:** nanoparticle · nanogap · Coulomb blockade · tunneling spectroscopy · quantum confinement

With the development of nanotechnologies, a variety of new synthetic methods of nanoparticles have been developed. Homogeneous nanoparticles, metallic,[1] semiconducting,[2] magnetic,[3,4] or even superconducting,[5,6] are now available, as well as heterogeneous systems such as core/shell nanoparticles,[7] mixing several types of materials.[8,9] To properly understand these materials, the characterization of their excitation spectra, the single electron level spectra, and the collective excitation spectra (phonon, magnons) is required.

Current tools for spectroscopic measurements include electron photoemission, various optical spectroscopic measurements from infrared to X-ray wavelengths, and neutron scattering. While those tools can be used to provide a wealth of information on bulk materials, they are poorly adapted for the study of nanoparticles. In contrast, electron tunneling spectroscopy is well adapted for the study of nanosized materials. The single electronic level spectrum can be measured with very high resolution through elastic tunneling spectroscopy,[10−12] while the collective excitation modes can be studied through inelastic tunneling spectroscopy.[13]

The tunneling electronic spectrum can be measured either with a scanning tunnel microscope (STM)[10,11] or "on-chip", where the nanoparticle is trapped between two electrodes separated by a gap of a few nanometers.[10,14−20] While some results have been obtained with both methods, they are difficult to implement. On one hand, STM requires extensive surface preparation of the substrate, the nanoparticle, and the tip and allows only a limited stability of the tunnel junction, which makes measurements of the inelastic tunneling spectrum challenging. Furthermore, it does not permit the presence of a gate, which is useful for the spectroscopy of nanosized objects that often are in the regime of a Coulomb blockade. On the other hand, the stability of on-chip spectroscopy is much better and can easily accommodate one or several gates; however, it requires the challenging step of trapping the nanoparticle

* Address correspondence to herve.aubin@espci.fr.

Received for review November 12, 2012 and accepted January 17, 2013.

**Published online January 17, 2013**
**10.1021/nn305264g**

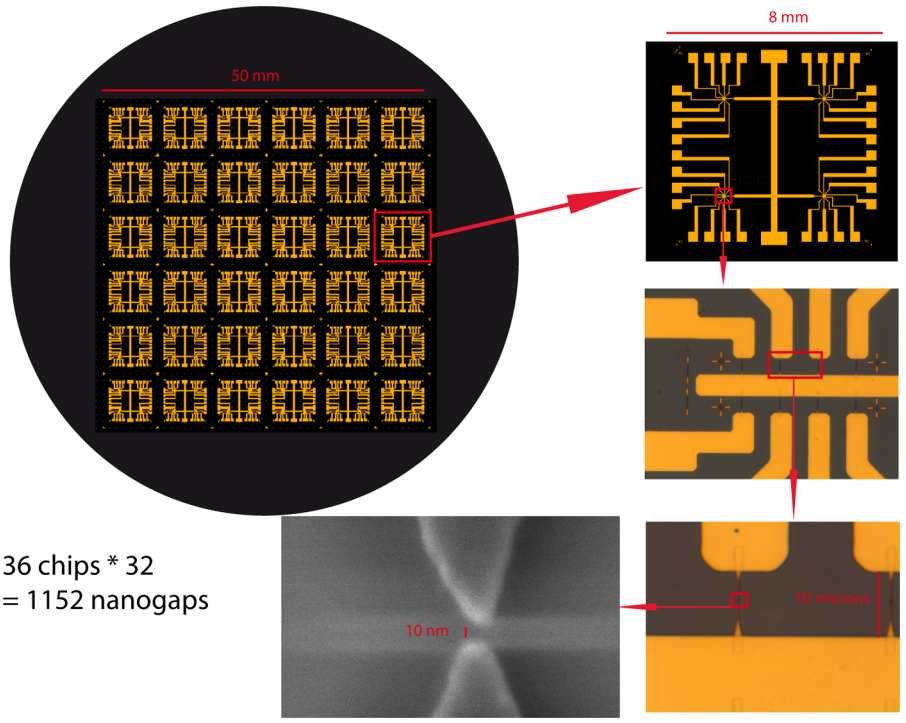


**Figure 1. Chip circuit on which are deposited the nanoparticles; 36 chips are fabricated on a 3 in. wafer. Each chip contains 32 nanogaps. The distance between the electrodes is in the 10−20 nm range.**

within the nanogap. In this work, we present a new method for trapping nanoparticles within nanometer-spaced electrodes. It allows a high success rate for nanoparticle trapping and allows the characterization of the nature of the current path that has been created, *i.e.* whether the current flows across a single nanoparticle or through a percolating path spanning many nanoparticles.

## RESULTS AND DISCUSSION

A typical chip circuit used for the study of nanoparticles is shown in Figure 1. The electrodes Cr(5 nm)/Au(25 nm) are deposited on a p-doped silicon substrate covered with a 200 nm thick silicon oxide layer. One chip of size 8 × 8 mm contains 32 nanogaps, *i.e.*, 32 drain electrodes separated from the common source electrode by a nanogap whose size is in the 10−20 nm range. The electrodes are patterned by e-beam lithography of a PMMA resist on a Vistec EBPG5000+, followed by the thermal evaporation of the electrodes and lift-off.

Trapping nanoparticles between nanometer-spaced electrodes has already been the subject of several works,[10,14−20] among which different methods have been explored. One common method, used with gold nanoparticles chemically synthesized with the Turkevich method, is to sink the chip in the nanoparticle solution for several hours, then to blow the chip dry and to measure the electronic current to test for the presence of nanoparticles within the nanogap. The success rate of this method of preparation is extremely low and requires the preparation of hundreds of samples before one with a single nanoparticle trapped within the nanogap can be obtained.

While several methods have been attempted to make the sample preparation more deterministic, such as dielectrophoretic trapping of the nanoparticles[14,18,21] or self-aligned nanolithography,[22] the trapping of the nanoparticles within the nanogap remains essentially a random process, where the deposition rate of the nanoparticles on the chip should be high enough so that trapping of the nanoparticle occurs during a reasonable amount of time, but not too high, to avoid the formation of a percolating path involving many nanoparticles, which would prevent the possibility of studying the electronic current across a single nanoparticle.

To describe the process of trapping nanoparticles, we revisit the percolation problem with nanometer-spaced electrodes through numerical simulation. The array used for the simulation is shown in Figure 2, where the nanoparticles and electrodes are represented by filled squares in an empty array. The closest distance between the electrodes is exactly one unit cell. Thus, the electrodes can be connected by a single nanoparticle falling in this cell. Before starting the simulation, a distribution of nanoparticles is prepared on the array with the occupation probability $p$ for one unit cell. The simulation starts from the left electrode, painting blue squares into red squares as they are met on the path. We repeat the simulation $N = 1000$ times for each value of $p$. At the end of each simulation indexed $i$ where $i = 1 \rightarrow 1000$, we record whether the

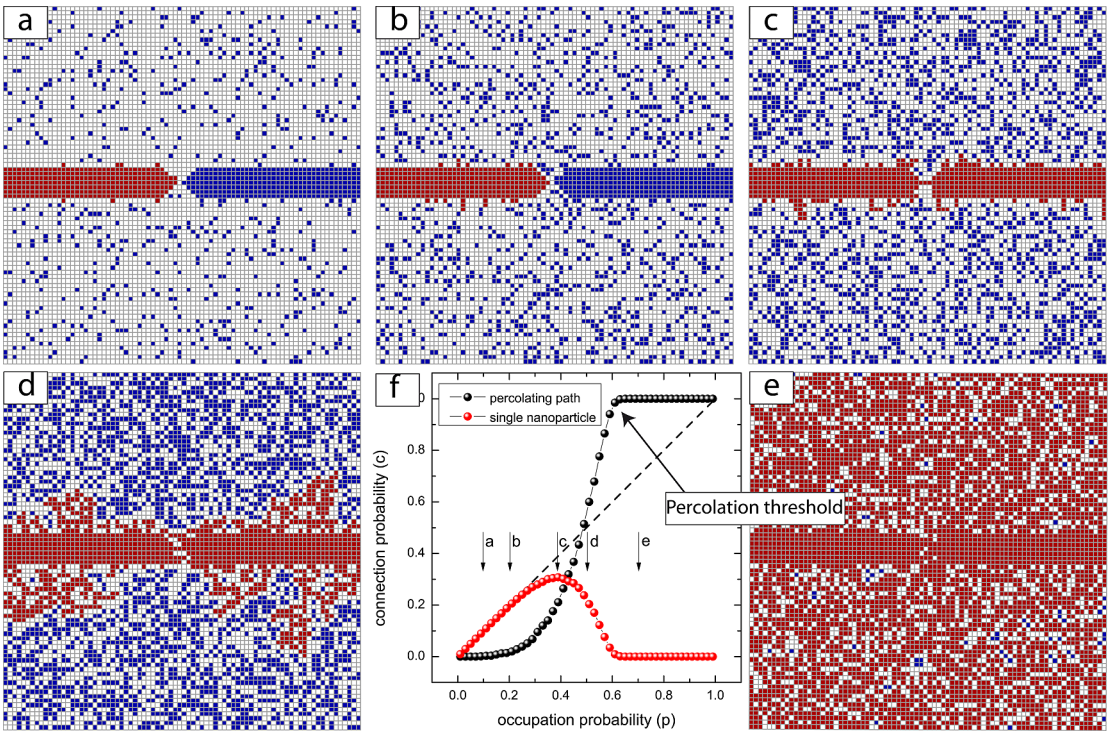


**Figure 2. Example arrays obtained from the simulation of the deposition of nanoparticles on the chip with nanometer-spaced electrodes. After deposition of the nanoparticles (blue squares), the simulation starts from the left electrode and the nanoparticles are painted in red as they are encountered on the path. The simulation stops when no more nanoparticles can be reached. When the two electrodes are disconnected, only the left electrode is red (a and b); when the two electrodes are connected, both electrodes are red (c–e). (f) Probability of the two electrodes of being connected, as function of occupation probability of the unit cell, by a single nanoparticle between the electrodes (dashed line) and by a percolating path across many nanoparticles (black dotted curve). The percolation threshold $p_c \simeq 0.6$, above which the electrodes are always connected, is clearly apparent on this last curve. The red dotted curve shows the probability of the electrodes of being connected by a single nanoparticle and no other percolating path. This curve has a maximum for an occupation probability $p \simeq 0.4$.**

two electrodes are connected ($c_i = 1$) or disconnected ($c_i = 0$). The average $c = \sum c_i/N$ gives the connection probability of the two electrodes for the occupation probability $p$. Figure 2f) shows the probability $c$ as a function of the occupation probability $p$ in three cases. In the first case, only one nanoparticle is allowed on the array, located exactly between the two electrodes, with the occupation probability $p$. In this case, the connection probability is simply given by the occupation probability, $c_{single} = p$, shown as a dashed line. In the second case, we start the simulation with a random distribution of nanoparticles deposited on the array without allowing for the presence of a nanoparticle between the electrodes. In this case, the two electrodes can be connected only through a percolating path involving several nanoparticles. The black dotted curve, Figure 2f), shows that the connection probability $c_{percolating}$ is weak at small $p$ but increases rapidly when $p \rightarrow p_c$ where $p_c \simeq 0.6$ is the percolation threshold. For $p > p_c$, a percolation path between the two electrodes can always be found and the electrodes are always connected, $c_{percolating} = 1$. The percolation threshold found here is close to the value found in previous studies of percolation in two-dimensional arrays.[23] From these last two curves, the probability of connecting the two electrodes with a single nanoparticle *and* in the absence of any other percolating path is given by $c = c_{single} \times (1 - c_{percolating})$, shown as a red dotted curve in the same figure. We find that this last curve has a maximum at $c_{max} \simeq 0.3$ for an occupation probability $p \simeq 0.4$.

This analysis formalizes the obvious statement that the samples should be prepared with a low occupation probability, *i.e.*, low sample coverage with nanoparticles, to avoid percolating current paths. This also implies that the connection probability will be necessarily low, $c_{max} \simeq 0.3$, implying that many samples have to be prepared before one is successfully obtained. As the preparation of hundreds of samples with low nanoparticle coverage is not a practical solution, we present here a new approach for the fabrication of chips with in-nanogap trapped nanoparticles. This method effectively permits making thousands of trials of nanoparticle trapping within only a few hours. Furthermore, as shown below, the method allows characterizing the type of current path that has been formed, *i.e.*, whether a single nanoparticle has been trapped or a percolating current path implying many nanoparticles has been formed. We applied the method to trap a single gold nanoparticle within a nanogap,

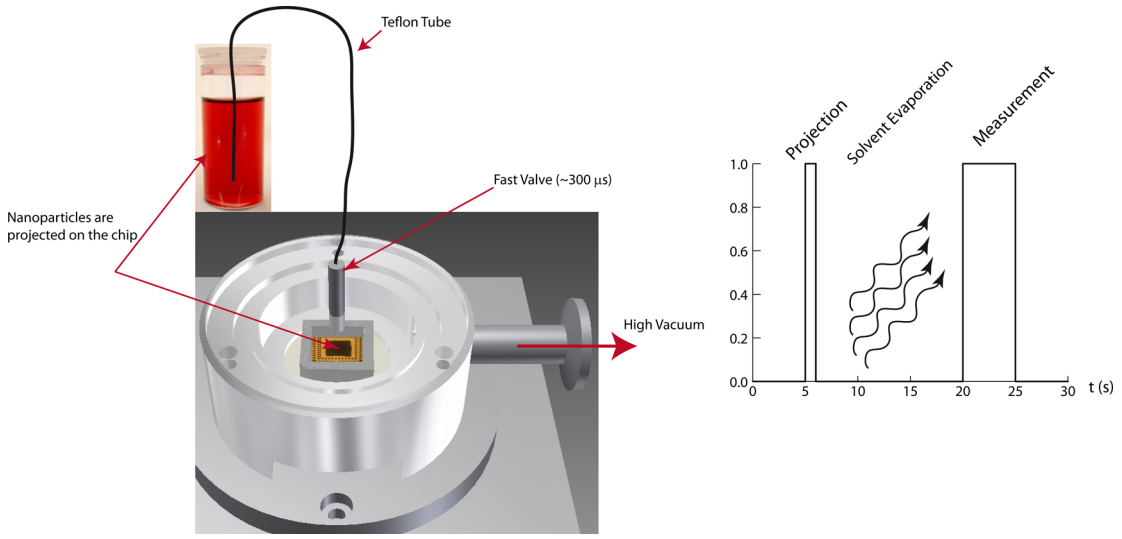


**Figure 3. (Left) High-vacuum chamber used for the projection of nanoparticles on the chip, using a fast pulsed valve. (Right) Sketch of the cycle. First, the nanoparticles in solution are projected onto the chip by opening the valve for a short time (<1 ms). Second, a delay between 10 and 20 s is observed, to allow for the full evaporation of the solvent. Third, the tunnel current is measured.**

which was tested by the observation of a Coulomb blockade.

After wired bonding of the chip on a 44-pin LDCC ceramic package, the chip circuit is checked for the presence of leaking currents between the source, drain electrodes, and the gate. Bias voltages on the source and the gate are applied with usual voltage source instruments, and the tunnel current across the nanogap is measured using a current to voltage amplifier with gain typically set to $10^9$ V/A. A scanning switch system is used to quickly probe the 32 drain electrodes. Leaking drain electrodes are discarded, and the measured tunnel current of the opened nanogap is typically below the noise level of the amplifier, which is about 1 pA measured on a bandwidth of 1 Hz.

As shown Figure 3, the chip circuit is installed in a small chamber, closed by a transparent acrylic cover, on top of which is fixed a fast pulsed valve. The setup is installed in a glovebox under argon to allow for the preparation of chips with air-sensitive nanoparticles. A solution of nanoparticles is prepared and poured in an Eppendorf; a small PTFE tube connects the Eppendorf to the valve. The chamber is pumped to high vacuum ($10^{-6}$ mbar). If needed, this chamber can be installed on a hot plate to help in solvent evaporation or, instead, can be fixed on the coldfinger of a cryostat.

After starting the acquisition software, the experiment proceeds along the following steps: opening of the valve for a short period (<1 ms), which leads to the projection of nanoparticles onto the chip; then a short delay (10 s) is observed, during which the solvent is evaporating; finally, the tunneling current between the source and drains is measured. If the measured electronic current is below the threshold value set into the acquisition software, the cycle (projection−delay−measure) is repeated, until the tunnel current exceeds the preset threshold.

As the full cycle is only about 30 s long, thousands of projection/measurements can be done within a single day. Obviously, the large quantity of cycles is the most important advantage of the method. It allows using weakly concentrated nanoparticle solutions, such that thousands of trials can be done before reaching the percolation threshold. This increases significantly the probability of detecting a connection due to the trapping of a single nanoparticle. The second remarkable feature offered by this method is to provide a means to test the type of current path formed. Indeed, the evolution of the current with time differs whether a single nanoparticle has been trapped or a percolating path involving many nanoparticles has been formed.

Starting from a blank chip with no current between the electrodes, Figure 4 shows the current, measured at a bias voltage of 0.1 V, as a function of time where each data point in the curve is measured 10 s after projecting the nanoparticles on the chip. In the first case, shown by the red dotted curve, the current remains equal to zero after each projection until the nanoparticle gets trapped in the nanogap, where the current suddenly jumps to a large value that stops the projection−delay−measure cycle. The setup was tested with gold nanoparticles synthesized by the Turkevich method.[24] The nanoparticles' size is in the range 10−15 nm. They are surrounded by citrate ligands, which provide them colloidal stability in water. The citrate ligands also form the tunnel barrier between the nanoparticle and the electrodes. With these gold

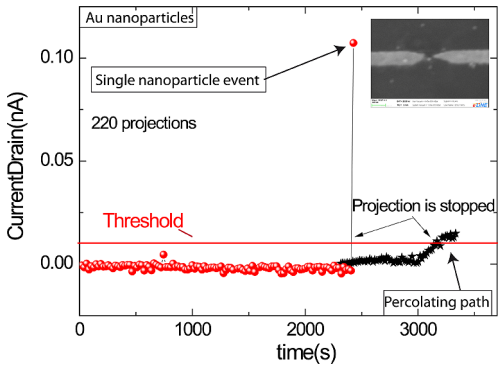


**Figure 4. Each data point of the red dotted curve corresponds to a measurement of the tunnel current following the projection of nanoparticles. When the measured tunnel current exceeds the threshold, the projection stops. When the current jumps abruptly from zero to a large finite value, this means that a single nanoparticle has been trapped within one nanogap. In contrast, when poorly conducting nanoparticles are used, the tunnel current only increases progressively as a thin film builds on the top of the chip (black stars). After the projection system stops upon reaching the current threshold, the current curve will look like either the red dotted curve, which corresponds to a single nanoparticle trapped, or the black starred curve, which corresponds to the formation of a percolating current path.**

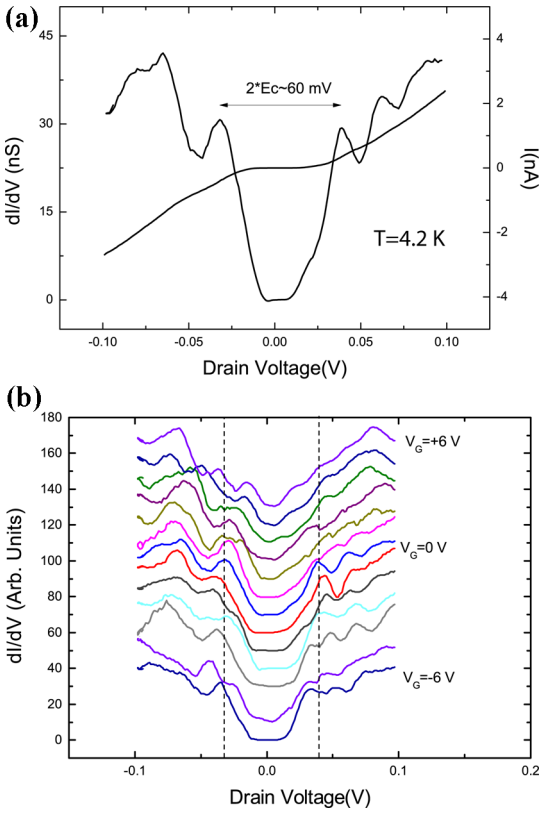


**Figure 5. (a) Current voltage ($I-V$) curve and corresponding derivative (d$I$/d$V$) curve for a single nanoparticle trapped within a nanogap, measured at the gate voltage $V_{Gate}$ = 0 V. The peaks observed in the d$I$/d$V$ curve is characteristic of a Coulomb blockade. Changing the gate voltage displaces the Coulomb blockade peaks as shown in (b).**

nanoparticles, we found that projection curves typical of single nanoparticle events could be easily obtained. Furthermore, we found that all samples prepared with such a projection curve displayed Coulomb blockade behavior, as shown in Figure 5. When other types of nanoparticles are used, the transparency of the tunnel barrier between the nanoparticle and the gold electrodes becomes a major issue. Indeed, many types of nanoparticles are synthesized in the presence of long-chain organic ligands that stabilize the nanoparticles during the synthesis. Furthermore, many nanoparticle systems are extremely air-sensitive and form an oxide layer in air. The organic layer and/or the oxide layer makes a thick insulating layer that prevents electron tunneling from/to the nanoparticle. While those issues can be partly solved, the organic layer can be replaced by smaller ligands using ligand exchange methods,[4,9,14,25−31] and the oxide layer can be avoided by operating the setup in a glovebox under argon. The poor tunnel barrier transparency is the most common cause for the sample preparation to fail. In our projection system, when nanoparticles covered with a thick insulating layer are used, the tunnel current does not jump abruptly as a nanoparticle gets trapped within the nanogap; instead, the electronic current increases progressively as a thin film of nanoparticles is deposited and current paths get formed, until the projection system stops when the current exceeds the preset threshold. Figure 4 shows an example of a projection curve that was obtained with poorly conducting $Fe_3O_4$ nanoparticles. We see that the current increases progressively until the threshold is reached, where the projection stops. When this type of curve is observed, there is no reason to believe that a single nanoparticle has been trapped and the sample can be discarded.

To check for the presence of a single nanoparticle within the nanogap, Figure 5 shows the current−voltage curve measured at low temperature ($T$ = 4.2 $K$) for the sample with the projection curve typical of single nanoparticle trapping shown Figure 4. The data display Coulomb blockade peaks in the conductance as a function of the drain voltage, which is characteristic of single-electron tunneling in a single nanoparticle. The distance between two peaks $\Delta V \simeq$ 30 mV corresponds to the charging energy $E_c = e^2/2C$ for one nanoparticle, where the self-capacitance is given by $C = 4\pi\varepsilon\varepsilon_0 r$, the nanoparticle radius $r \simeq 7$ nm, and $\varepsilon$ = 3.9 is the dielectric coefficient of silicon oxide. Furthermore, we find that the Coulomb blockade peaks are shifted with the gate bias voltage, as expected.

While the Coulomb gap can be observed in transport properties of nanoparticle films,[32−35] the observation of Coulomb peaks in the conductance as a function of drain voltage can be considered as the signature of transport within a single nanoparticle.[14,17,36] After transport property measurements, the samples are

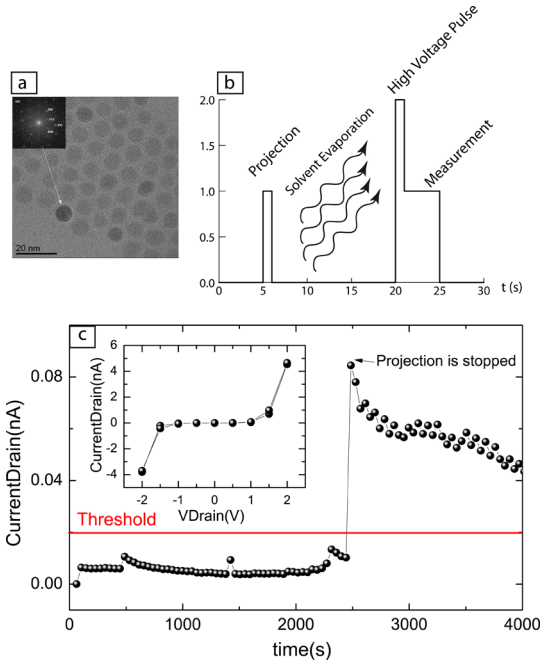


**Figure 6. (a) TEM image of an assembly of undecanoic acid-capped $Fe_3O_4$ nanoparticles. Inset: Power spectrum of the particle indicated by the arrow. (b) Cycle (projection–evaporation–pulse–measure). (c) Main panel: Projection curve. Inset: Current–voltage (*I*–*V*) curve for the prepared sample.**

checked by scanning electron microscopy, as shown in Figure 4.

In addition to gold nanoparticles, we applied the projection method to a variety of other nanoparticles. We found that, in our conditions, it was not possible to prepare conducting samples from CdSe or $Bi_2Te_3$ nanoparticles, either with organic ligands or an exchanged ligand using previously published methods.[26] Past reports on transport properties of CdSe nanoparticles by STM[12] or deposited as thin films[29] highlight the importance of thermal annealing of nanoparticles in a vacuum before such measurements can be done. Indeed, the thermal annealing step is required to eliminate the residual surfactant ligands, which makes the tunnel barrier between the nanoparticle and the electrodes more transparent. These works suggest that our projection setup could be improved by projecting the nanoparticles on the chip at high temperature and in an ultrahigh vacuum.

Finally, we also attempted the preparation of samples with magnetite $Fe_3O_4$ nanoparticles. Undecanoic acid-capped $Fe_3O_4$ nanoparticles of an average size of about 10 nm (Figure 6a) are obtained by the reaction of iron(III) acetylacetonate in benzyl alcohol at 175 °C followed by a ligand exchange process as previously described.[37] The ligand exchange process permits reducing the size dispersion and the obtainment of a stable colloidal solution in a nonpolar solvent (*e.g.*, hexane). The nanoparticles are highly crystalline and single crystalline, as demonstrated by the power spectrum in the inset of Figure 6a. The undecanoic acid was further exchanged using $NOBF_4$ in DMF following the protocol described in refs 25, 26, and 38 and the Supporting Information. When these nanoparticles are deposited, they form only poorly conducting nanoparticle films. The projection curve is of the percolating path type, as shown in Figure 4. Numerous works[39–41] have shown that oxygen vacancies can be created in metal oxides by the application of a large electric field. As oxygen vacancies are n-type dopants, this leads to electric-field-induced transition from insulator to metal, the so-called switching in current–voltage characteristics. As the last projection curve suggests that the nanoparticles actually are insulating, we added, in the projection–delay–measure cycle described above, an additional step where a voltage pulse of 3 V is applied. Using only this procedure, we found projection curves corresponding to single-nanoparticle trapping events, as shown in Figure 6. This observation suggests that nominally synthesized $Fe_3O_4$ nanoparticles were actually insulating, probably due to oxidation as shown by XPS measurements, Figure S1 in the Supporting Information. However, by applying voltage pulses, this creates the oxygen vacancy dopants, which allows the observation of electronic transport in those nanoparticles.

## CONCLUSION

To summarize, starting with a discussion of the percolation problem applied to the trapping of nanoparticles between nanometer-spaced electrodes, we show that a good strategy to trap single nanoparticles is to prepare samples with a low coverage of nanoparticles on the chip to avoid percolating current paths. This implies the preparation of many samples in order to increase the probability of successful trapping. To that end, we presented a new method where nanoparticles are projected in-vacuum on the chip, followed by a measure of the tunnel current. As the number of projections can be as large as a few thousand, the probability of trapping successfully a single nanoparticle becomes close to 1. A plot of the tunneling current as function of time can discriminate between the two current paths possible, *i.e.*, a single nanoparticle trapped between the electrodes or a percolating path across many nanoparticles. While gold nanoparticles synthesized in water offer a clean system for the trapping of single nanoparticles and the study of single-electron transport in nanoparticles, they do not oxidize and are free of organic ligands. Many nanoparticle systems synthesized in organic solvents actually are very air sensitive, are prone to develop an oxide layer, and often are covered by an organic ligand layer, which makes it difficult to predict the conductance of the nanoparticle trapped within the nanogap. In this context, the projection method described here

presents a significant advantage, as it allows assessing whether a single nanoparticle has been trapped within the nanogap or a percolative conducting film has been formed.

## METHOD

**Ligand Exchange of Magnetite Nanoparticles.** $NOBF_4$ and DMF were used as purchased from Sigma Aldrich. In 500 $\mu$L of DMF, we add 10 $\mu$L of $NOBF_4$. To this solution we add 500 $\mu$L of the magnetite nanoparticles dispersed in hexane. After shaking for several minutes, phase transfer of the nanoparticles from nonpolar solvent to the polar solvent is observed. Then, the DMF containing the nanoparticles is extracted and mixed with hexane/toluene (50/50) to precipitate the nanoparticles. The solution is centrifuged, the supernatant is removed, and the particles are redispersed in $CH_2Cl_2$. This protocol is repeated three times to wash the nanoparticles. Finally, the nanoparticles are dispersed in DMF. Infrared spectroscopy could not show characteristics peaks of organic ligands located about 3000 $cm^{-1}$, indicating that organic ligands were successfully exchanged with the shorter $BF_4$ ligands.

*Conflict of Interest:* The authors declare no competing financial interest.

*Acknowledgment.* We acknowledge support from ANR grant "QUANTICON" 10-0409-01 and ANR grant "CAMELEON" 09-BLAN-0388-01.

*Supporting Information Available:* XPS spectrum of $Fe_3O_4$ nanoparticles. This material is available free of charge *via* the Internet at http://pubs.acs.org.

## REFERENCES AND NOTES


1. Brust, M.; Walker, M.; Bethell, D.; Schiffrin, D. J.; Whyman, R. Synthesis of Thiol-Derivatised Gold Nanoparticles in a Two-Phase Liquid-Liquid System. *J. Chem. Soc., Chem. Commun.* **1994**, 801–802.
2. Murray, C. B.; Norris, D. J.; Bawendi, M. G. Synthesis and Characterization of Nearly Monodisperse CdE (E = Tulfur, Selenium, Tellurium) Semiconductor Nanocrystallites. *J. Am. Chem. Soc.* **1993**, *115*, 8706–8715.
3. Black, C. T. Spin-Dependent Tunneling in Self-Assembled Cobalt-Nanocrystal Superlattices. *Science* **2000**, *290*, 1131–1134.
4. Sun, S. Monodisperse FePt Nanoparticles and Ferromagnetic FePt Nanocrystal Superlattices. *Science* **2000**, *287*, 1989–1992.
5. Zolotavin, P.; Guyot-Sionnest, P. Meissner Effect in Colloidal Pb Nanoparticles. *ACS Nano* **2010**, *4*, 5599–5608.
6. Resa, I.; Moreira, H.; Bresson, B.; Mahler, B.; Dubertret, B.; Aubin, H. Synthesis of Monodisperse Superconducting Lead Nanocrystals. *J. Phys. Chem. C* **2009**, *113*, 7120–7122.
7. Hines, M. A.; Guyot-Sionnest, P. Synthesis and Characterization of Strongly Luminescing ZnS-Capped CdSe Nanocrystals. *J. Phys. Chem.* **1996**, *100*, 468–471.
8. Shevchenko, E. V.; Bodnarchuk, M. I.; Kovalenko, M. V.; Talapin, D. V.; Smith, R. K.; Aloni, S.; Heiss, W.; Alivisatos, A. P. Gold/Iron Oxide Core/Hollow-Shell Nanoparticles. *Adv. Mater.* **2008**, *20*, 4323–4329.
9. Lee, J.-S.; Shevchenko, E. V.; Talapin, D. V. Au-PbS Core-Shell Nanocrystals: Plasmonic Absorption Enhancement and Electrical Doping via Intra-Particle Charge Transfer. *J. Am. Chem. Soc.* **2008**, *130*, 9673–9675.
10. Petta, J. R.; Salinas, D. G.; Ralph, D. C. Measurements of Discrete Electronic States in a Gold Nanoparticle using Tunnel Junctions Formed from Self-Assembled Monolayers. *Appl. Phys. Lett.* **2000**, *77*, 4419–4421.
11. Overgaag, K.; Liljeroth, P.; Grandidier, B.; Vanmaekelbergh, D. Scanning Tunneling Spectroscopy of Individual PbSe Quantum Dots and Molecular Aggregates Stabilized in an Inert Nanocrystal Matrix. *ACS Nano* **2008**, *2*, 600–606.
12. Sun, Z.; Swart, I.; Delerue, C.; Vanmaekelbergh, D.; Liljeroth, P. Orbital and Charge-Resolved Polaron States in CdSe Dots and Rods Probed by Scanning Tunneling Spectroscopy. *Phys. Rev. Lett.* **2009**, *102*, 196401.
13. Hansma, P. K. *Tunneling Spectroscopy: Capabilities, Applications, and New Techniques*; Plenum Press, 1982; Vol. 9; p 493.
14. Khondaker, S. I.; Luo, K.; Yao, Z. The Fabrication of Single-Electron Transistors Using Dielectrophoretic Trapping of Individual Gold Nanoparticles. *Nanotechnology* **2010**, *21*, 095204.
15. Nishino, T.; Negishi, R.; Kawao, M.; Nagata, T.; Ozawa, H.; Ishibashi, K. The Fabrication and Single Electron Transport of Au Nano-Particles Placed Between Nb Nanogap Electrodes. *Nanotechnology* **2010**, *21*, 225301.
16. Bolotin, K. I.; Kuemmeth, F.; Pasupathy, A. N.; Ralph, D. C. Metal-Nanoparticle Single-Electron Transistors Fabricated Using Electromigration. *Appl. Phys. Lett.* **2004**, *84*, 3154–3156.
17. Kuemmeth, F.; Bolotin, K. I.; Shi, S.-F.; Ralph, D. C. Measurement of Discrete Energy-Level Spectra in Individual Chemically Synthesized Gold Nanoparticles. *Nano Lett.* **2008**, *8*, 4506–4512.
18. Khondaker, S. I.; Yao, Z. Fabrication of Nanometer-Spaced Electrodes Using Gold Nanoparticles. *Appl. Phys. Lett.* **2002**, *81*, 4613–4615.
19. Park, H.; Lim, A. K. L.; Alivisatos, A. P.; Park, J.; McEuen, P. L. Fabrication of Metallic Electrodes with Nanometer Separation by Electromigration. *Appl. Phys. Lett.* **1999**, *75*, 301–303.
20. Bezryadin, a.; Dekker, C.; Schmid, G. Electrostatic Trapping of Single Conducting Nanoparticles Between Nanoelectrodes. *Appl. Phys. Lett.* **1997**, *71*, 1273–1275.
21. Kumar, S.; Seo, Y.-K.; Kim, G.-H. Manipulation and Trapping of Semiconducting ZnO Nanoparticles into Nanogap Electrodes by Dielectrophoresis Technique. *Appl. Phys. Lett.* **2009**, *94*, 153104.
22. Lin, Y.-C.; Bai, J.; Huang, Y. Self-Aligned Nanolithography in a Nanogap. *Nano Lett.* **2009**, *9*, 2234–2238.
23. Stauffer, D. A. *Introduction to Percolation Theory*; Taylor & Francis: London, 1991.
24. Turkevich, J.; Stevenson, P. C.; Hillier, J. A Study of the Nucleation and Growth Processes in the Synthesis of Colloidal Gold. *Discuss. Faraday Soc.* **1951**, *11*, 55–75.
25. Dong, A.; Ye, X.; Chen, J.; Kang, Y.; Gordon, T.; Kikkawa, J. M.; Murray, C. B. A Generalized Ligand-Exchange Strategy Enabling Sequential Surface Functionalization of Colloidal Nanocrystals. *J. Am. Chem. Soc.* **2011**, *133*, 998–1006.
26. Nag, A.; Kovalenko, M. V.; Lee, J.-S.; Liu, W.; Spokoyny, B.; Talapin, D. V. Surface Ligands. *J. Am. Chem. Soc.* **2011**, *133*, 10612–10620.
27. Kovalenko, M. V.; Bodnarchuk, M. I.; Talapin, D. V. Nanocrystal Superlattices with Thermally Degradable Hybrid Inorganic-Organic Capping Ligands. *J. Am. Chem. Soc.* **2010**, *132*, 15124–15126.
28. Kovalenko, M. V.; Bodnarchuk, M. I.; Zaumseil, J.; Lee, J.-S.; Talapin, D. V. Expanding the Chemical Versatility of Colloidal Nanocrystals Capped with Molecular Metal Chalcogenide Ligands. *J. Am. Chem. Soc.* **2010**, *132*, 10085–10092.
29. Talapin, D. V.; Lee, J.-S.; Kovalenko, M. V.; Shevchenko, E. V. Prospects of Colloidal Nanocrystals for Electronic and Optoelectronic Applications. *Chem. Rev.* **2010**, *110*, 389–458.
30. Kovalenko, M. V.; Scheele, M.; Talapin, D. V. Colloidal Nanocrystals with Molecular Metal Chalcogenide Surface Ligands. *Science* **2009**, *324*, 1417–1420.
31. Voitekhovich, S. V.; Talapin, D. V.; Klinke, C.; Kornowski, A.; Weller, H. CdS Nanoparticles Capped with 1-Substituted

5-Thiotetrazoles: Synthesis, Characterization and Thermolysis of Surfactant. *Chem. Mater.* **2008**, *20*, 4545–4547.
32. Moreira, H.; Yu, Q.; Nadal, B.; Bresson, B.; Rosticher, M.; Lequeux, N.; Zimmers, A.; Aubin, H. Electron Cotunneling Transport in Gold Nanocrystal Arrays. *Phys. Rev. Lett.* **2011**, *107*, 176803.
33. Parthasarathy, R.; Lin, X.-M.; Jaeger, H. Electronic Transport in Metal Nanocrystal Arrays: The Effect of Structural Disorder on Scaling Behavior. *Phys. Rev. Lett.* **2001**, *87*, 186807.
34. Parthasarathy, R.; Lin, X.-M.; Elteto, K.; Rosenbaum, T.; Jaeger, H. Percolating through Networks of Random Thresholds: Finite Temperature Electron Tunneling in Metal Nanocrystal Arrays. *Phys. Rev. Lett.* **2004**, *92*, 076801.
35. Tran, T.; Beloborodov, I.; Lin, X.; Bigioni, T.; Vinokur, V.; Jaeger, H. Multiple Cotunneling in Large Quantum Dot Arrays. *Phys. Rev. Lett.* **2005**, *95*, 076806.
36. Yang, P.; Arfaoui, I.; Cren, T.; Goubet, N.; Pileni, M.-P. Unexpected Electronic Properties of Micrometer-Thick Supracrystals of Au Nanocrystals. *Nano Lett.* **2012**, *12*, 2051–2055.
37. Pinna, N.; Grancharov, S.; Beato, P.; Bonville, P.; Antonietti, M.; Niederberger, M. Magnetite Nanocrystals: Nonaqueous Synthesis, Characterization, and Solubility. *Chem. Mater.* **2005**, *17*, 3044–3049.
38. Rosen, E. L.; Buonsanti, R.; Llordes, A.; Sawvel, A. M.; Milliron, D. J.; Helms, B. A. Exceptionally Mild Reactive Stripping of Native Ligands from Nanocrystal Surfaces by Using Meerwein's Salt. *Angew. Chem., Int. Ed.* **2012**, *51*, 684–689.
39. Kim, T. H.; Jang, E. Y.; Lee, N. J.; Choi, D. J.; Lee, K.-J.; Jang, J.-t.; Choi, J.-s.; Moon, S. H.; Cheon, J. Nanoparticle Assemblies as Memristors. *Nano Lett.* **2009**, *9*, 2229–2233.
40. Yang, J. J.; Pickett, M. D.; Li, X.; Ohlberg, D. A. A.; Stewart, D. R.; Williams, R. S. Memristive Switching Mechanism for Metal/Oxide/Metal Nanodevices. *Nat. Nanotechnol.* **2008**, *3*, 429–433.
41. Odagawa, A.; Katoh, Y.; Kanzawa, Y.; Wei, Z.; Mikawa, T.; Muraoka, S.; Takagi, T. Electroforming and Resistance-Switching Mechanism in a Magnetite Thin Film. *Appl. Phys. Lett.* **2007**, *91*, 133503.